Microstructure and Mechanical Properties of Spray Formed and Hot Pressed/Heat Treated Al-(20-30 wt%) Mg2Si-2% Cu Alloy

Goudar DM[1*], Srivastava VC[2], Rudrakshi GB[3]

[1]Tontadarya College of Engineering, Gadag -582101, India

[2]Basaveshwar Engineering College, Bagalkot-562101, India

[3]National Metallurgical Laboratories, Jamshedpur -831 007, India

Research Article

ABSTRACT

In the present investigation, Al-(20-30%wt) Mg_2Si-2Cu alloys were synthesized by spray forming process and further processed by hot pressing for densification. The alloys were further subjected to age hardening heat treatment. The spray formed, age hardened and as-cast alloys were characterized by microstructure and mechanical properties. The microstructure of spray formed alloys exhibited finer and evenly distributed primary β-Mg_2Si particles and θ-Al_2Cu phase and clusters of discrete and high volume fraction of Q-phase. As-cast alloys mainly consist of large sized polygonal primary β-Mg_2Si, coarse Chinese script of Al_2Cu and needle shaped eutectic Q-phase. Hot pressing of the spray formed alloy promotes the microstructural refinement, reduction in porosity, fragmentation and redistribution of secondary phases. Artificial age hardened alloys exhibits the large quantity of θ-Al_2Cu precipitates less than 2 μm size uniformly distributed in the matrix. The β phase re-precipitates in a very fine spherical form results in an increase in the area fraction of β-Mg_2Si phase during aging. The significant enhancement in ultimate strength in heat treated and sprays formed alloys as compared to the as-cast alloy. The SEM of fracture surfaces of tensile specimens was taken on spray formed age hardened and as cast alloys. The fractographs revealed the transformation from brittle mode to ductile dimples.

INTRODUCTION

The hypereutectic Al-Si alloys with alloying elements such as Mg, Cu, Fe and Mn have been successfully produced by modern processing technologies to improve strength to weight ratio, mechanical properties and wear behavior at elevated temperature [1]. Alloying of Al with high content of Mg and Si results in the formation of Mg_2Si phase and eutectic Al-Mg-Si phase. Offers the possibility of significant decrease in density (density of Mg_2Si-1.99 gcm^{-3}) and increase in stiffness compared to other Al alloys and makes them superior material for the light weight automotive applications [2]. However, the slow cooling rate of the melt associated with conventional casting methods results in a coarse microstructure of primary phase and formation of large intermetallic phases with a high degree of micro-macro segregation. Al alloy with high content of Mg_2Si poses several difficulties by conventional casting processes due to excessive slag formation and generation of porosity caused by high solubility of hydrogen

in the melts [3]. The materials with low density in combination with outstanding mechanical and wear properties require alternate production techniques. The spray atomization and deposition, also known as spray forming, is one of such processes combining two different but integral steps of melt atomization and deposition. This has inherent rapid solidification effect, semi-solid state, near net shape processing capability [4]. The spray forming has attracted considerable interest as a viable process for manufacturing of alloys, composites and structural materials with the benefits associated with the rapid solidification such as fine grained microstructure, increased solid solubility, fine primary and secondary phases [5]. Hence, the products have enhanced material properties viz, strength, wear resistance and ductility. Compared to conventional casting techniques, the Mg_2Si content can be increased substantially in spray forming which leads to new light alloy systems. Further improve the wear resistance by addition of Cu to Al-Mg-Si alloy by heat treatment [6]. In the present investigation, Al-20Mg$_2$Si-2Cu, Al-25Mg$_2$Si-2Cu and Al-30Mg$_2$Si-2Cu alloys are produced by spray forming (SF). The new lightweight alloys have been studied with respect to microstructure, hardness, and tensile properties. The effect of heat treatment on the microstructure, mechanical behavior of hot pressed spray formed (SF+HP) alloys were studied and the same has been compared with SF and as-cast alloys.

EXPERIMENTAL DETAILS

The Al-20Mg$_2$Si-2Cu, Al-25Mg$_2$Si-2Cu and Al-30Mg$_2$Si-2Cu alloys were synthesized by spray forming process. The nominal compositions of alloys and details of the process parameters employed used in the present investigation are shown in the **Tables 1 and 2**.

Table 1. Nominal Chemical compositions of (wt.%) alloys

Alloy	Si	Fe	Mn	Mg	Cu	Ni	Al
Al-20Mg$_2$Si-2Cu	7.39	0.7	0.04	11.8	1.80	0.24	Bal
Al-25Mg$_2$Si-2Cu	9.23	0.8	0.04	15.3	1.77	0.20	Bal
Al-30Mg$_2$Si-2Cu	10.86	0.5	0.05	19.3	1.84	0.20	Bal

Table 2. Details of spray forming process parameters.

Alloy	Super heat melt temp (ºC)	Substrate distance (mm)	Gas pressure (MPa)	Melt flow rate (Kg min^{-1})
Al-(20-30) wt% Mg$_2$Si-2Cu	150	400	0.45	2.2

The finite amount of porosity is invariably present in the SF alloys. Keeping this in view SF alloys were subjected to hot pressing. Samples were prepared by cutting from the central region of the deposit were heated at 490ºC-510ºC kept in a furnace for 2 hour and hot pressed at a temperature of 480°C and pressure of 55 MPa by 100-Ton hydraulic press. The tensile tests were carried out at a crosshead speed of 0.5 mm/min^{-1} which corresponds to a nominal strain rate of 0.05 min^{-1}. The samples of SF alloys were subjected to age hardening heat treatment after hot pressing. The age hardening treatment was accomplished as per ASM handbook (ASM, 1997). Heat treatment process was carried out in a muffle resistance furnace with a temperature accuracy of ±3°C. The cycle of heat treatment comprises of solutionizing at 510ºC with a soaking time of 2 h, quenching in an ice-cold water bath and aging at 210°C for 2 h.

The density measurements were carried out on cylinder samples of diameter 10 mm and 50 mm length prepared from the centre portion of the perform of SF samples before and after hot pressing by a water displacement method as per ASTM: B962-08. Porosity measurements were carried out by preparing samples of 5 × 10 × 10 mm size from the centre portion of the preform by vacuum Xylene Impregnated Method. The X-Ray diffraction analysis was carried out on a pan analytical Philips system (Model: MCRS 2000-3). This system has a Cu-Kα anode (λ=0.154065 nm) and 482 kW sealed tube operated at 160 kV and 20 mA. The step size and step time is 0.01 and1°/sec respectively. The observed d-values were compared with corresponding peaks given in JCPDS files. The samples of the as-cast, SF, SF+HP and age hardened alloys were prepared using standard metallographic techniques and polished samples were etched with Keller's reagent. The microstructures of samples were examined under a ZEISS Optical Microscope and grain size measurement was carried out as per ASTM E-112-96 (ASTM, 2003). The chemical compositions of the constituent present in phases were examined using an energy dispersive X-ray (EDX) micro-analyzer. The SEM was operated at an acceleration voltage of 10-30 Kv.

The microstructure, fracture surface of the tensile specimens, worn surface and wear debris were examined on SEM (Model: JEOL JSM-6480LV). Micro hardness measurements were carried using Vickers hardness tester (Model: MVH, Meta-tech Industries, India) using an indentation load of 300 g and allowing a dwell time of 15 seconds for each indentation. Each micro-hardness

value reported in the present work is an average value of five readings. Standard tensile specimens were prepared and tested by following the ASTME-8 standard (ASTM, 2000).

RESULTS AND DISCUSSIONS

Microstructure

Figure 1 shows the X-ray diffraction pattern of SF alloys. The XRD pattern confirms the presence of primary Al, Mg_2Si second phase with a ratio 3:1 and Al_2Cu and Q as a third phase in the alloys. Furthermore, the obtained diffract grams demonstrate that the peak intensities of the Mg_2Si increase with the increase of the amount of Mg_2Si. The strongest diffraction peak of primary Mg_2Si phase of SF alloy corresponds to the (220) plane. This indicates the crystalline growth of primary Mg_2Si phase in SF alloy.
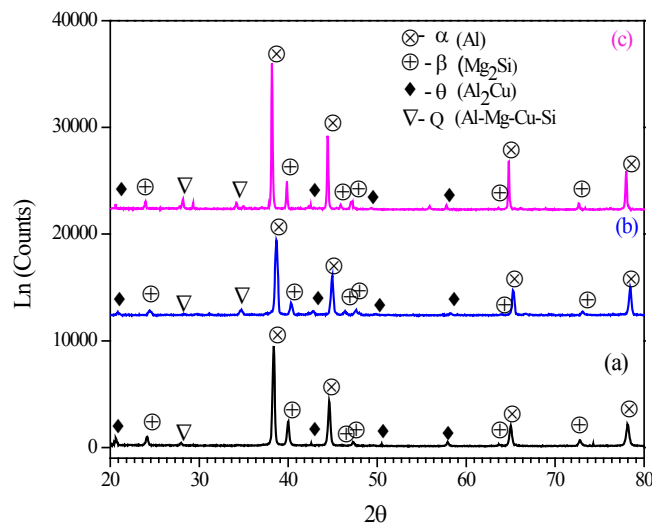

Figure 1. X-ray diffraction pattern of spray formed,(a)Al-20Mg$_2$Si-2Cu (b) Al-25Mg$_2$Si-2Cu and (c) Al-30Mg$_2$Si-2Cu alloys.

Figure 2 shows the SEM/EDS micrograph of as-cast alloys. It consists of coarse primary Mg_2Si phase, Al_2Cu phase and quaternary compound Q-$Al_2Cu_2Mg_8Si_7$ phase in the form of intertwined structure. These phases are distributed randomly in the Al-matrix of dendrite network structure. The mole ratio of Mg-Si phase is close to 1.7, indicating the Mg_2Si phase exists in an irregular plate-like/vermiform and sizes in the range of 50-270 μm. The Mg_2Si phase is found as primary as well as a part of the eutectic matrix, thus, revealing two different morphologies. The presence of Cu leads to the formation of θ-Al_2Cu intermetallics in white contrast exists in the form of Chinese script as well as irregular and long acicular structure of Q-$Al_6Mg_{41}Si_{34}Cu_9$ phase. The elemental composition of different phases in the alloys as shown in the **Tables 3-5**.
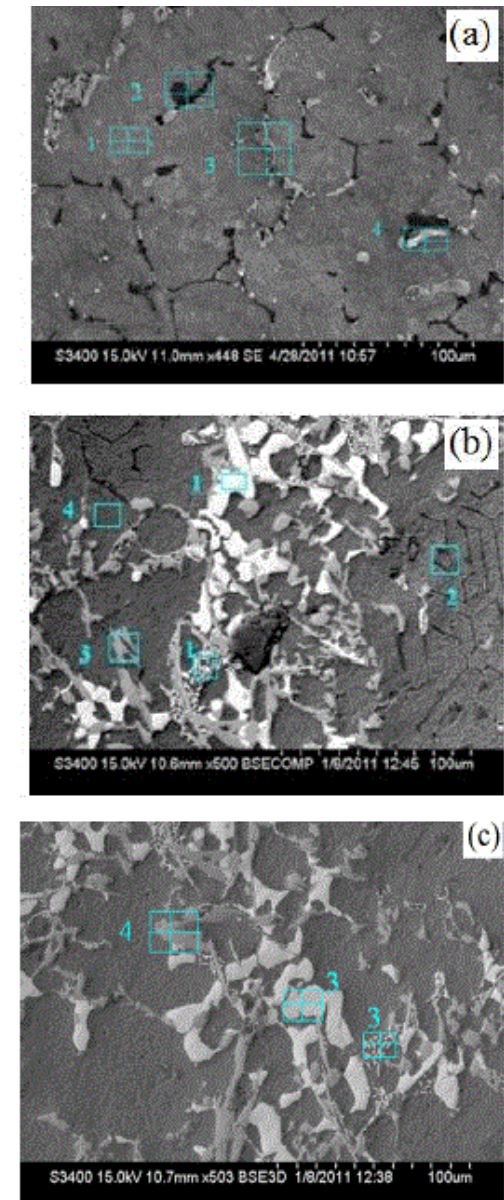
Figure 2. SEM/EDS micrograph of as-cast alloys, (a) Al-0Mg$_2$Si-Cu, (b) Al-25Mg$_2$Si-2Cu And (c) Al-300Mg$_2$Si-2Cu[6].

Table 3. Phase chemical composition (wt%) of Al-20Mg$_2$Si-2Cu as-cast alloy.

Location	Phase	Al-k	M-kg	Si-k	Cu-k
Point 1	α-Al96	93.98	2.69	2.03	1.34
Point 2	β-Mg$_{66}$Si$_{34}$	2.02	60.75	35.68	--
Point 3	θ-Al$_{72}$Cu$_{19}$	52.17	0.56	0	32.86
Point 4	Q-Al$_{16}$Mg$_{41}$Si$_{34}$Cu$_9$	14.38	33.44	31.86	19.4

Table 4. Phase chemical composition (wt%) of as-cast Al-25Mg$_2$Si-2Cu alloy.

Point	Phase 1	Al-k	Mg-k	Si-k	Cu-k	Fe-k
Point-1	θ-Al$_{64}$Cu$_{32}$	64.23	1.24	2.34	31.96	0.23
Point-2	β-Mg$_{57}$Si$_{33}$	3.96	54.86	33.42	0.12	0.15

| Point-3 | Q-Al$_2$Cu$_2$Mg$_2$Si$_7$ | 34.95 | 37.28 | 8.20 | 19.80 | 00.16 |
| Point 4 | α-Al | 96.23 | 0.34 | 2.34 | 0.56 | 0.04 |

Table 5. Phase chemical compositions of as-cast Al-30Mg$_2$Si-2Cu alloy.

Location	Phase	Al-k	Mg-k	Si-k	Cu-k
Point-1	α-Al	94.5	0.26	0.59	1.60
Point-2	β-Mg$_{64}$Si$_{34}$	1.7	59.0	36.2	0.00
Point-3	θ-Al$_{65}$Cu$_{25}$	48.3	5.02	4.31	42.0
Point-4	Q-Al$_{24}$Mg$_{43}$Si$_{26}$Cu$_7$	23.0	35.2	25.0	16.5

Figure 3 show the SEM/EDS micrograph of SF alloys. It consists of fine and uniformly distributed primary β-Mg$_2$Si particles (dark color) having size in the range between 2 to 5 μm, small volume fraction of particulates of θ-Al$_2$Cu phase (in white contrast) and a small volume fraction of Q-Al$_{34}$Cu$_8$Mg$_{30}$S$_{27}$ phase (dark grey) exists in the form of clusters of discrete particles.
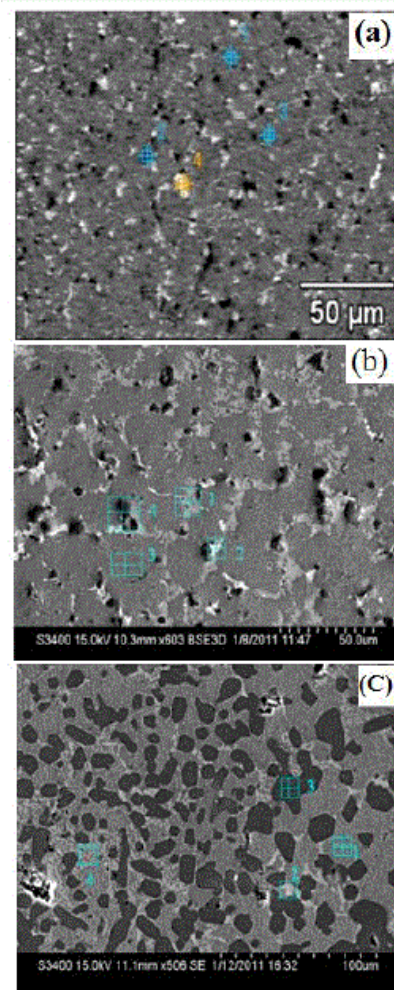

Figure 3. SEM/EDS micrographs of SF alloys (a) Al-20Mg$_2$Si-2Cu,(b) Al-25Mg$_2$Si-2Cu and (c) Al-30Mg$_2$Si-2Cu alloy [6].

Uniformly distributed primary β-Mg$_2$Si particles crystallize from the melt and grow in the faceted form and develops various round edge polygonal shapes. The elemental composition of different phases in the alloys is shown in the **Tables 6-8**. The optical micrgraphs of SF alloys are shown in **Figure 4**. The non-connected spherical form (black contrast) of pores of size in the range of

20 to 50 μm distributed uniformly in the matrix. The average (% of volume) porosity in the SF before and after hot pressing are given in the **Table 9**. The density of SF alloys varied from 91% to 93.4%. The density of SF alloys after hot pressing varies from 95.4% to 96.3%. It is also observed from the results that the density of alloys decreases with increase in Mg_2Si content approximately by 3% with an increase of Mg_2Si content in the alloy. The SEM micrographs of the SF+HP alloys are shown **Figure 5**. The microstructures show the reduction of porosity, fragmentation of Mg_2Si particles and partial recrystallization of secondary phases ('θ' and 'Q') to fine particles. The presences of coarse block like Mg_2Si phase of as-cast alloys. Due to slow cooling rate and broad temperature interval between the liquidus and solidus at higher Mg_2Si content in the pseudo binary section of the phase diagram will cause castings with a coarse microstructure of Mg_2Si phase as well as the eutectic constituents [7].

Table 6. Phase chemical composition (wt.%) of SF Al-20Mg$_2$Si-2Cu alloy.

Location Point	Phase	Al-k	Mg-k	Si-k	Cu-k
Point-1	α-Al	94.5	0.26	0.59	1.60
Point-2	β-Mg$_{64}$Si$_{34}$	1.7	59.0	36.2	0.00
Point-3	θ-Al$_{65}$Cu$_{25}$	48.3	5.02	4.31	42.0
Point-4	Q-Al$_{24}$Mg$_{43}$Si$_{26}$Cu$_7$	23.0	35.2	25.0	16.5

Table 7. Phase chemical composition (wt%) of SFAl-25Mg$_2$Si-2Cu alloy.

Point	Phase	Al-k	Mg-k	S-k	Cu-k	Fe-k
Point-1	Q-Al$_{12}$Mg$_{64}$Si$_{17}$Cu$_7$	11.03	54.7	16.60	15.66	--
Point-2	θ-Al$_{69}$Cu$_{28}$	55.43	0.16	2.2	41.76	0.15
Point-3	α-Al	91.65	0.18	6.11	1.2	0.12
Point-4	β-Mg$_2$Si	1.45	58.9	35.98	2.30	0.051

Table 8. Phase chemical composition (wt%) of SFAl-30Mg$_2$Si-2Cu alloy.

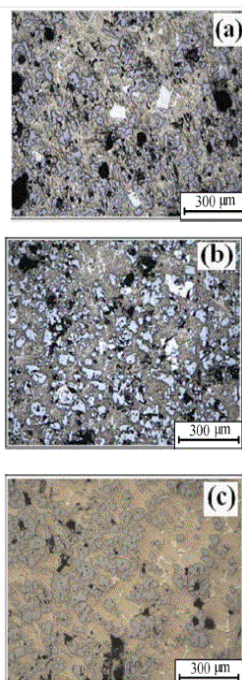| Points	Phase	Al-k	Mg-k	Si-k	Cu-k
Point-1	α-Al$_{98}$	96.01	1.36	0.72	1.89
Point-2	Q-Al$_{28}$Mg$_{34}$Si$_{28}$Cu$_9$	25.58	27.98	26.59	18.56
Point-3	β-Mg$_{67}$Si$_{31}$	1.69	62.91	34.21	0.00
Point-4	θ-Al$_2$Cu	43.25	5.02	5.11	41.01

Figure 4. Optical micrographs of the SF alloys (a) Al-20Mg$_2$Si-2Cu, (b) Al-25Mg$_2$Si-2Cu and (c) Al-30Mg$_2$Si-2Cu.
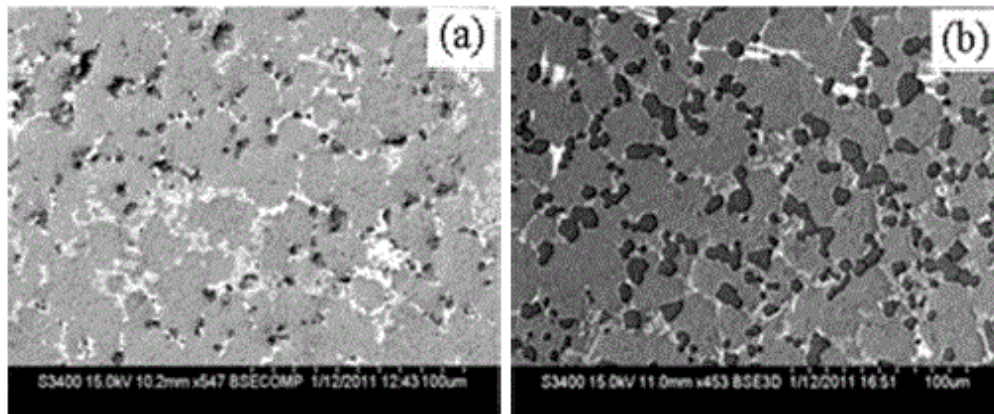
Figure 5. SEM micrographs of SF+HP alloys (a) Al-20Mg$_2$Si-2Cu and (b) Al-30 Mg$_2$Si-2Cu [6].

Table 9. Density and porosity values of SF and hot pressed alloys.

Alloy	Theoretical Density (gmcm^{-3})	Density of SF alloy (gcm^{-3})	Density of SF+HP alloy (gcm^{-3})	Average porosity of SF alloy (%)	Average porosity of SF+HP alloy (%)
Al-20Mg$_2$Si-2Cu	2.535	2.33 (91%)	2.42 (95.4%)	13.56%	4.5
Al-25Mg$_2$Si-2Cu	2.482	2.26 (91%)	2.38(95.8%)	16.23%	6.23
Al-30Mg$_2$Si-2Cu	2.428	2.25 (93.4%)	2.34(96.3%)	14%	6.56

In spray forming process, the solidification phenomena changes due to the effect of high cooling rate during the atomization stage and the unique microstructural evolution mechanism during deposition. Due to rapid solidification rate, there is a possibility of increase in the concentration of alloying elements beyond the equilibrium solubility in the matrix. Further, the formation of metastable phases and very fine microstructures in SF alloys. During atomization and flight stage, the droplets experience large under cooling prior to nucleation of primary Mg$_2$Si phase, leading to an extensive microstructural refinement. Thus, large amount of fine, uniformly distributed primary Mg$_2$Si particles and greater number of precipitates (θ-Al$_2$Cu phase, Q phase) are formed in the supersaturated Al-matrix. Increasing of cooling rate is associated with an increase in under cooling of the melts which in turn refines the size of microstructures as well as changes the sequence of solidification [8]. In addition, the relatively rapid solidification restricts the grain growth and yields fine structures.

High the under cooling during solidification of droplets in the atomization stage, the nucleation rate of β-(Mg$_2$Si) phase increases and growth rate is suppressed [9]. Because of high content of Mg and Si large number of agglomerated Mg$_2$Si particles can be observed in spray formed Al-30Mg$_2$Si-2Cu alloy. During deposition, small particles which agglomerate together are assumed to be one large particle. The initial size of Mg$_2$Si phase depends significantly on the spray deposition conditions. The evolution and amount of porosity is mainly depends on the thermal state of the atomized droplets and their impingement on the substrate [10]. If the liquid fraction of the deposition surface is too high, gas can be entrapped which leads to spherical pores. If the deposit surface is too cold, the gaps formed by impinging particles cannot be filled which also leads to cold porosity. Thus, amount and form of porosity in spray deposit is strongly governed complex interaction of process parameters like melt superheat and is a, G/M ratio and flight distance.

Hot pressing process leads to fragmentation and redistribution of primary phases and dissolution of some of the precipitate phases during the process. It is obvious from the micrographs that the individual grain is more prominent and intermetallic phases and the elements 'in the solution are fast precipitated at the grain boundaries. The presence of small precipitates of 'θ' and 'Q' phases in SF alloy subjected to preheat treatment before deformation process make the microstructure more uniform. The severe stress imposed by hot-pressing generates high density dislocations in the grains. Subsequently the movement and arrangement of dislocation forms lot of small angle grain-boundaries refining initial grains into several substructure. In addition to the refinement of grains, hot deformation also promotes homogeneous precipitation hardening of 'θ' and Q-phases which can pin the movement of dislocations to restrain grain coarsening during re-crystallization effectively [11]. No significant difference is observed in the other microstructural features such as the aspect ratio and distribution of brittle 'β' particles. **Figure 6** represents the SEM micrograph of solution heat treated alloys. It can be observed from the micrographs that most of the secondary phases ('θ' and 'Q') are dissolved in the α-Al matrix which results in increased super saturation in the matrix. It is observed from the microstructure that the spheriodised Mg$_2$Si phase and large amount Q-(Al$_{49}$-Mg$_{19}$-Si$_{27}$ Cu$_8$) phase precipitates are found around the Mg$_2$Si phase interface (Point 2).
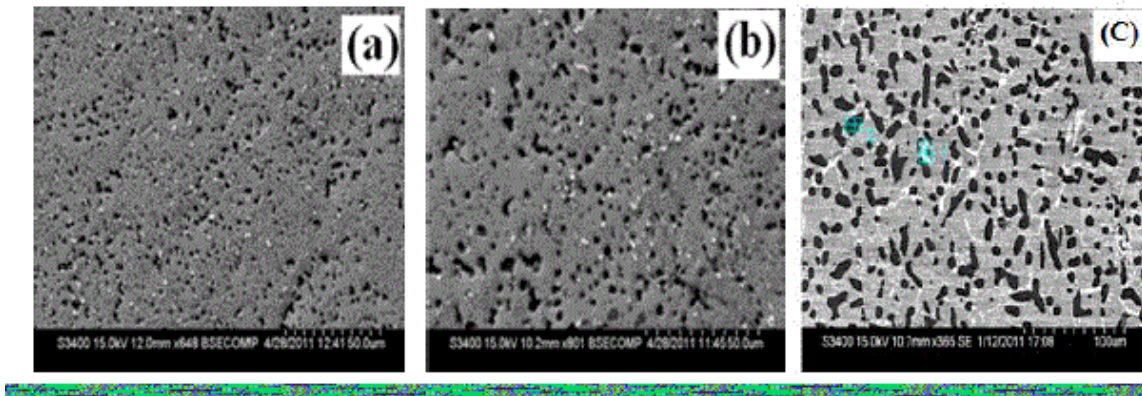
Figure 6. SEM micrographs of SF+HP+ Solution heat treated (SH) alloys (a) Al-20Mg$_2$Si-2Cu, (b) Al-25Mg$_2$Si-2Cu and (c) Al-30Mg$_2$Si-2Cu [6].

The Mg and Cu rich phases which are formed during solidification are dissolved into α-Al matrix. **Table 10** Shows the elemental chemical composition of different phases in the solution treated Al-30Mg$_2$Si-2Cu alloy. **Figure 7** shows the SEM micrographs of SF+HP and artificial age hardened alloys. It can be seen that a large quantity of θ-Al$_2$Cu (white contrast) precipitates less than 2 µm size uniformly distributed in the matrix. The β phase re-precipitates in a very fine spherical form results in an increase in the area fraction of β-Mg$_2$Si phase during aging. Increase of Al-Mg$_2$Si eutectic phase and area fraction of precipitation along the interface of primary Mg$_2$Si (β) phase can be clearly observed in artificial aged Al-30Mg$_2$Si-2Cu. Chemical composition of Mg$_2$Si and Al$_2$Cu phases in age hardened alloy is shown in the **Table 8**. The spheroidization of Mg$_2$Si phase during solution heat treatment is due to the fragmentation of Mg$_2$Si branches or smoothing of particle corners. Further, Al-matrix gets supersaturated due to re-dissolution of Mg and Cu rich phases into α-Al matrix. Due to quenching, the solute components are retained in an unstable state in the solid solution and large number of dislocations and vacancies are created at the boundaries of Mg$_2$Si particles and also the Al/Mg$_2$Si interface possessing high dislocation density. As a result, morphological change of Mg$_2$Si particles and considerable amount of 'Q' phase precipitates are formed around the grain boundaries of Mg$_2$Si phase [12]. When the samples are quenched from the solutionzing temperature, point defects and line defects are formed around the Mg$_2$Si particles due to large thermal stress generated by the significant difference of thermal expansion coefficients between Mg$_2$Si and Al. These defects serve as the nucleation sites of precipitates promoting the precipitation [13]. Because of the larger amounts of Mg$_2$Si particles in the spray-formed alloy, the number of the nucleation sites for precipitates are more. The θ-phase leads to the formation of disordered clusters of atoms under solution treatment. These clusters are named Guinier-Preston (GP) zones and are coherent to the surrounding matrix. Under artificial ageing these GP zones begin to transform to 'θ' and this is still coherent. As the aging continues the 'θ' phase promote precipitation of a finer dispersion of the semi-coherent 'θ' phase. When the peak aging time is achieved, the θ-phase will become an incoherent equilibrium 'θ' phase. It is observed in the **Figure 7** that the fine and uniform distribution of Al$_2$Cu and 'Q' phases in the α-Al matrix also increase area fraction of fine Mg$_2$Si phase.
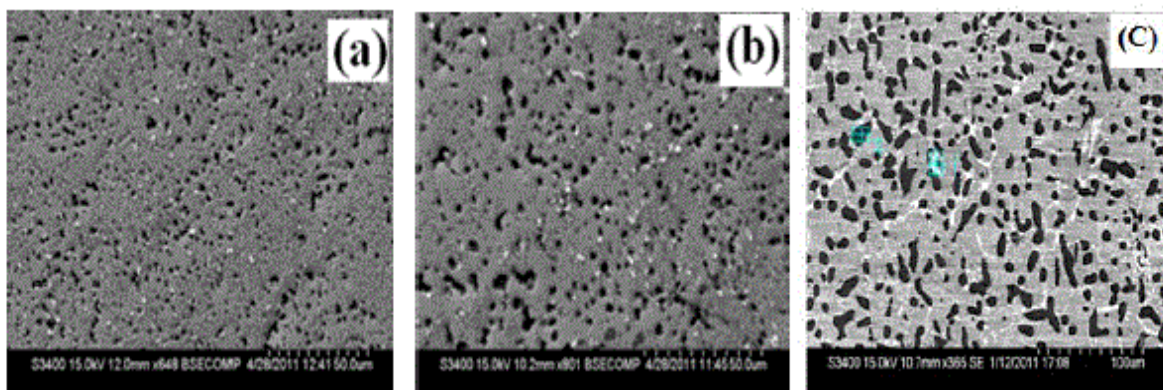

Figure 7. SEM micrograph of SF+HP + age hardened alloys (a) Al-20Mg$_2$Si-2Cu, (b) Al-25Mg$_2$Si-2Cu and a Al-30Mg$_2$Si-2Cu lloy [6].

Table 10. Compositions different of phases of age hardened Al-30Mg$_2$Si-2Cu alloy.

Point	Phase	Mg	Al	Si	Cu
Point 1	β-Mg$_2$Si	63.79	0.61	34.02	--
Point 2	θ-Al$_2$Cu	10.14	43.24	5.02	39.98

The fine Mg_2Si phase combined with the Al_2Cu precipitates can significantly increase the strength of the alloy. Upon additional aging the particles grow with an increase in coherency strain until interfacial bond strength is exceeded and they become incoherent. Once all the solute atoms have segregated from the supersaturated solid solution the precipitates will continue to grow in accordance with the Ostwald ripening. Coarsening of the larger precipitates occur by dissolution of the smaller precipitates. The coarsening is driven by the reduction of surface energy [14].

MECHANICAL PROPERTIES

Hardness

The results of micro hardness measurements are sown in the **Table 11** Compared with as-cast alloy, the hardness of SF+HP alloys increased significantly. Furthermore, the hardness increases linearly with increase in Mg_2Si content of the alloy. From the comparative study of hardness it is clear that the artificial age hardened alloys exhibits nearly 2 times and 1.5 times high hardness as compared to as-cast and SF+HP alloys.

Table 11. Micro hardness of as-cast, SF+HP and age hardened alloys.

Alloy	Processing condition	Hardness (Hv)
Al-20Mg$_2$Si-2Cu	As-cast	69 ±1.62
Al-25Mg$_2$Si-2Cu	As-cast	78 ±2.06
Al-30Mg$_2$Si-2Cu	As-cast	86 ±1.61
Al-20Mg$_2$Si-2Cu	SF+HP	110 ±1.74
Al-25Mg$_2$Si-2Cu	SF+HP	126 ±2.64
Al-30Mg$_2$Si-2Cu	SF+HP	132 ±1.54
Al-20Mg$_2$Si-2Cu	Age hardened	154 ±1.84
Al-25Mg$_2$Si-2Cu	Age hardened	163 ±1.56
Al-30Mg$_2$Si-2Cu	Age hardened	176 ±1.74

The increase in the hardness of SF+HP alloy is due to the partial recrystallization, fragmentation and redistribution of primary Mg_2Si phase, precipitation of fine θ, Q phases and reduced porosity due to hot pressing. The high volume fractions of uniformly dispersed hard β-particles greatly increase the flow stress and provide an appreciable impediment to plastic deformation. The increase in the hardness with increase in Mg_2Si content, this is due of the presence of larger amount of fine Mg_2Si particles, fine particulates of θ-Al_2Cu and Q phases. These phases will obstruct the movement of dislocations more efficiently and more difficult for plastic deformation to proceed. Increasing Mg_2Si content in the alloy leads to an increase in hardness and is in agreement with that of other investigators [15]. Increase in the hardness of age hardened alloys can be attributed to the increasing solubility of magnesium silicate markedly with solution treatment time resulting in a higher amount of dissolved Mg_2Si in Al-matrix. Solubility of Cu in the Al-matrix increases with solution treating temperature. During quenching, this Mg-Si and Cu is retained in solution. As a result, the Al phase contains Mg-Si and Cu in a supersaturated solid solution at room temperature. During aging, fine particles of Mg_2Si and Al_2Cu form and precipitate in the solution. Also, the sphreridiozation of Mg_2Si particles obtained during age hardening processing could lower the stress concentration at the interface of Mg_2Si particles and α-Al matrix.

Consequently the tendencies to initiate the subsurface cracks decrease hence increase in the hardness [16]. During aging the precipitates of Al_2Cu at the grain boundaries of primary Mg_2Si phase strongly strengthens the α-Al matrix there by increasing the bonding between Mg_2Si phase and the matrix resulting very high hardness in the aged alloy due to higher resistance of the matrix to plastic flow [17]. During the subsequent ageing and precipitation treatment at 220°C for 2h the solute atoms are rejected and formed new phases as Al_2Cu fine precipitate. The presence of the strained field around the new phases will limit the movement of dislocations, which can result in the increase in strength and hardness. Thus, the higher hardness of artificial age hardening alloys is clearly due to the high concentration of β-Mg_2Si and θ-Al_2Cu meta stable pre phases and super saturated Al-matrix As the aging time increased hardness decreased because precipitates transformed gradually from met stable state to the stable state, and finally to an incoherent interface between precipitates and matrix. According to Ostwald ripening, all the solute atoms gets segregated from the supersaturated solid solution and coarsening of precipitates by dissolution of the smaller precipitations due to reduction of surface energy. When the precipitates become large and few, the distance between the precipitates increases, therefore surface easier for the dislocations to pass through and resulting in a decrease in shear stress and therefore hardness [18].

Tensile Properties

Tensile properties of as-cast, SF+HP and artificially aged alloys are shown in **Table 12**. It is worth noting that the tensile

strength of SF+HP alloys is superior to the as-cast alloys but the ductility decreases. The tensile strength and ductility of SF+HP Al-20Mg$_2$Si-2Cu alloy shows 32.3% and 32.29% higher values than that of as-cast alloy. Compared with the SF+HP and as-cast alloys the UTS of age hardened alloy shows 1.67 and 2.50 times higher than the corresponding values for SF+HP and as-cast alloys. It is observed from the results that there is a significant decrease in elongation of age-hardened alloys as compared to that of as-cast and SF+HP alloys. SEM Morphology of tensile fracture surface of as-cast samples are shown in **Figure 8**. The fractured surfaces of as-cast alloys exhibit typical cleavage-fracture mode which is formed by the fracture and cracking of Mg$_2$Si particle and their peeling off from the Al-matrix. The fractured surfaces include clusters of considerably large sized voids, which are more or less locally distributed.

Table 12. Mechanical properties of as-cast, SF+HP and age hardened alloys.

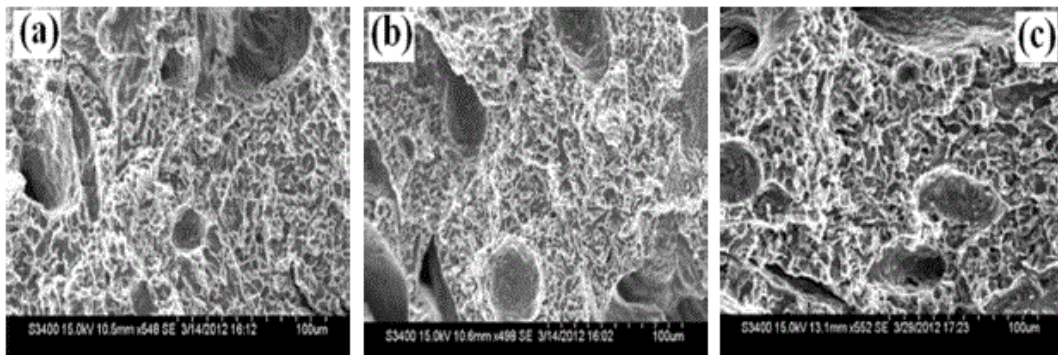| Alloy	Processing condition	UTS (MPa)	Elongation (%)
Al-20Mg$_2$Si-2Cu	As-cast	110	6.92
Al-25Mg$_2$Si-2Cu	As-cast	117	6.2
Al-30Mg$_2$Si-2Cu	As-cast	126	5.12
Al-20Mg$_2$Si-2Cu	SF+HP	164	3.79
Al-25Mg$_2$Si-2Cu	SF+HP	178	3.32
Al-30Mg$_2$Si-2Cu	SF+HP	216	3.26
Al-20Mg$_2$Si-2Cu	Heat treated	274	1.24
Al-25Mg$_2$Si-2Cu	Heat treated	290	1.32
Al-30Mg$_2$Si-2Cu	Heat treated	325	1.01

Figure 8. Tensile fracture surface of as-cast alloys (a) Al-20Mg$_2$Si-2Cu, (b) Al-25Mg$_2$Si-2Cu and (c) Al-30Mg$_2$Si-2Cu.
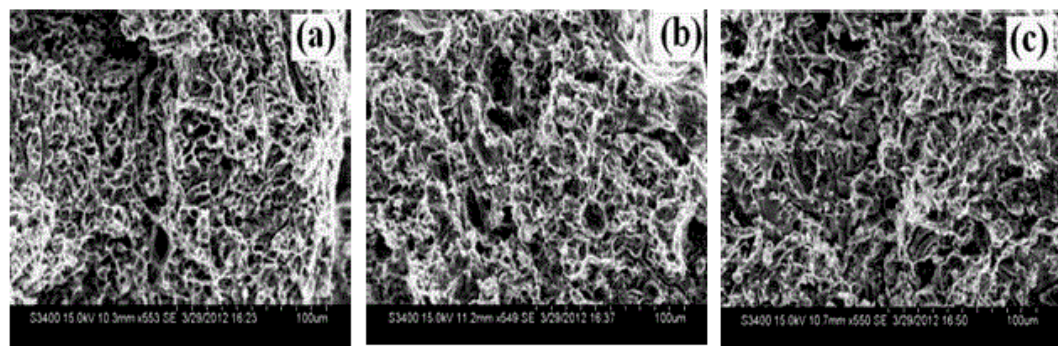

Figure 9. Tensile fracture surface of SF+ HP alloys (a) Al-20Mg$_2$Si-2Cu, (b) Al-25Mg$_2$Si-2Cu and (c) Al-30Mg$_2$Si-2Cu.
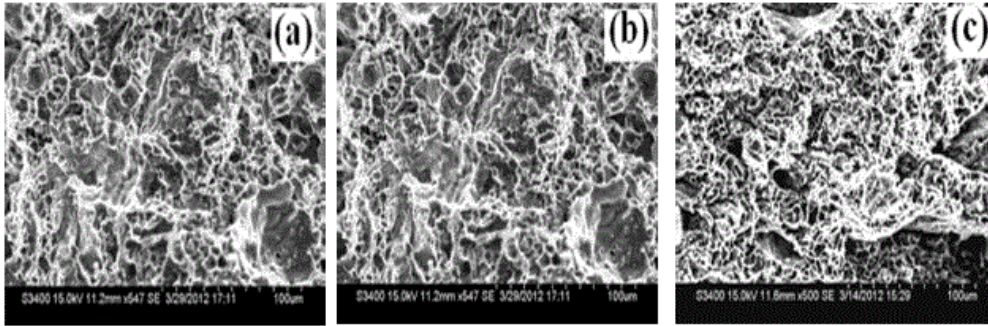
Figure 10. Tensile fracture surface of SF+HP and age hardened alloys (a) Al-20Mg$_2$Si-2Cu, (b) Al-25Mg$_2$Si-2Cu and (c) Al-30Mg$_2$Si-2Cu.

The fractographs of SF and hot pressed alloys are shown in **Figure 9**. It can be seen that the alloys reveals mixed mode of fracture by void nucleation and growth, as indicated by the general dimpled structure of the fracture surface. However, in the SF+HP alloys some pockets of brittle fracture with featureless, cleavage-like appearance suggesting pockets of brittle fractures are observed. The fracture of SF+HP alloys depicts reveals small and poorly defined facets connected by tear ridges or shallow dimples within the facets. A slight river pattern can also be seen radiating from the facet center. Predominant quasi-cleavage areas, suggesting that the brittle fracture mechanism has become dominant. From the fractographic observations, it is apparent that a drastic drop in ductility is connected with the embrittlement and cleavage of Mg$_2$Si phase. The fractographs of age hardened alloys is shown in **Figure 10**. It is observed from the fracture surfaces that all the alloys fail in brittle manner as characterized by the faceted nature of the fracture surfaces and large amount of equiaxed dimples along with cracked Mg$_2$Si particles at the bottom of dimples. This suggests that the uniformly distributed and fine equiaxed Mg$_2$Si particles may be helpful to improve the tensile strength.

The typical dendritic microstructure of the as-cast alloy has 'β' phase particle in polyhedral shape with sharp edges. In addition, Q and θ-phases exist in vermiform long acicular shapes and are unevenly distributed in α-Al matrix that results in inferior mechanical properties. During tensile testing of the as-cast alloy, damage appears by cracking of the θ-and Q-phases at small plastic strain [19]. As the strain progresses, small cracks and also some voids occur between the Mg$_2$Si particles. Then these defects coalesce to generate a crack that propagates along the Mg$_2$Si particles, which offer less resistance to crack propagation. This is due to their poor bonding with matrix as compared to the interdendritic regions.

The potential improvement in mechanical behavior in the SF+HP alloys may be attributed to the refined and equiaxed grain microstructure, sharply decreased segregation, increased metastable solid solubility and greater volume fraction of Mg$_2$Si intermetallics obtained during spray deposition process [20]. In the SF+HP alloys the intermetallics appear in the form of fine particles uniformly distributed in the matrix, which serve as the nucleation sites of voids reducing the resistance of the cavitations of the matrix and also causing the connection of micro voids in a shorter interval of time [21].

Both of these effects decreased the ductility of the SF+HP alloys. The heat treated alloys exhibit the high ultimate tensile strength and the low elongation.. There is a significant difference in the aspect ratio of the Mg$_2$Si and rounded Mg$_2$Si particles (smaller aspect ratio) in the heat treated condition promote an increase in the UTS due to the lower levels of stress concentration on the tip of the Mg$_2$Si particles which delay the fracture process. The increase in the strength of the alloy after the age hardening process is also attributed to the effects of fine 'Q' and Al$_2$Cu precipitates in the matrix. During the deformation, the precipitates restrict the movement of dislocation and the dislocation density increases around these precipitates which increase the flow stress during the deformation. The decrease in elongation after the heat treatment may be related with the mechanism of the growth of micro voids. The controlled ageing of solution treated alloys yield higher strength [21]. The fracture surfaces of all as-cast, SF+HP and artificially aged alloys reveal that the cracks seem to be initiated and propagated through the Mg$_2$Si intermetallics as well as the Al$_2$Cu and 'Q' phases of the alloys.

CONCLUSIONS

1. The microstructure of spray formed alloys exhibited finer and evenly distributed primary β-Mg$_2$Si particles and θ-Al$_2$Cu phase and a high volume fraction of Q-phase exist in the form of clusters of discrete particles. As-cast alloys mainly consist of large sized polygonal primary Mg$_2$Si, coarse Chinese script of Al$_2$Cu and needle shaped eutectic Q-phase. Hot pressing of the deposit promotes the microstructural refinement, reduction in porosity, fragmentation and redistribution of secondary phases. Artificial age hardened alloys a large quantity of θ-Al$_2$Cu precipitates less than 2μm size uniformly distributed in the matrix. The β phase re-precipitates in a very fine spherical form results in an increase in the area fraction of β-Mg$_2$Si phase during aging.

2. The hardness of the SF+HP alloys shows 60% higher than their as-cast alloys and increases with increasing M$_{g2}$Si content.

Heat treated alloys reaches to a value of around 200% more that of the as-cast alloys. The maximum hardness of age hardened alloys was attributed to the effects of small spacing between Mg_2Si particles, larger amounts of quenched-in defects, smaller grains associated with a massive precipitation of intermediate 'θ' and 'Q' phases in the matrix.

3. The tensile properties of SF+HP and Age hardened alloys exhibit higher UTS and low value of elongation compared to their as-cast counterparts alloys and UTS increases with increasing Mg_2Si content in both the SF+HP and the as-cast alloys. The fracture surface of all the SF+HP alloys exhibit typical cleavage-fracture mode and fractured samples of as-cast alloy show large facets with small dimples indicating a mixed mode of ductile and brittle fractures. Age hardened alloys exhibits faceted nature with large amount of equiaxed dimples and cracked Mg_2Si particles.

REFERENCES

1. Ibrahim Kurt H and Oduncuoglu M. Formulation of the Effect of Different Alloying Elements on the Tensile Strength of the in situ Al-Mg_2Si Composites. Metals 2015;5:371-382.

2. Frommeyer G, et al. Microstructure and Mechanical Properties of Mechanically Alloyed intermetallic Mg2Si-Al Alloys. J Metall 1994;pp:372-377.

3. Hummert K, et al. Industrially produced spray compacted Al alloys. Metall 1999;9:496-500.

4. Lavernia EJ and Yue Wu. Spray atomization and deposition. John Wiley& Sons Inc., New York 1996;pp:487-489.

5. Grant PS. Spray forming. J Progr Mater Sci 1995;39:497-508.

6. Goudar DM, et al. Effect of secondary processing on the microstructure and wear behavior of spray formed Al-30Mg2Si-2Cu alloy. J Mater Design 2013;47:489-496.

7. Ellendt N, et al. Spray forming of Mg2Si-rich Aluminum alloys. J Mater Sci Forum 2007;534-536:437-440.

8. Kang M, et al. Effect of Solidification Behavior on Microstructures and Mechanical Properties of Ni-Cr-FeSuperalloy investment Casting. J Materials (Basel) 2017;10:250.

9. Breta LA, et al. Microstructure and mechanical properties of spray deposited and extruded/heat treated hypoeutectic Al-Si alloy. J Mater Sci Eng A 2007;449-451:850-853.

10. Hu H, et al. On the Evolution of Porosity in Spray-Deposited Tool Steels. J Metall Mater Trans A 2000;31:725.

11. Goudar DM, et al. Effect of copper and iron on the wear properties of spray formed Al-28Si alloy. J Mater Design 2013;51:383-390.

12. Stelling O, et al. New spray formed Aluminium-Silicon-copper alloys with high Mg2Si content. Proceedings of the Conference on Spray deposition and Melt Atomization (SDMA) 2006.

13. Edwards GA, et al. The Precipitation Sequence in Al-Mg-Si Alloys. J Acta Mater 1998;46:3893-3904.

14. Li YJ, et al. Influence of Cu on the mechanical properties and precipitation behavior of AlSi7Mg Alloy during aging treatment. J Scripta Mater 2006;54:99-103.

15. Wang G, et al. Influence of Cu content on ageing behavior of AlSiMgCu cast alloys. J Mater Design 2007;28:1001-1005.

16. Chaudhury SK and Apelian D. Fluidized Bed Heat Treatment of Cast Al-Si-Cu-Mg Alloys. J Metall Mater Trans A 2006;37:2295-2311.

17. Song Y and Baker TN. A calorimetric and metallographic study of precipitation process in AA6061 and its composites. J Mater Sci Eng A 1995;201:251-260.

18. Aiza Jaafar, et al. Effects of Composition on the Mechanical Properties and Microstructural Development of Dilute 6000 Series Alloys. J Appl Sci 2012;12:775-780.

19. Shabestari SG and Moemeni H. Effect of Cu and solidification conditions on microstructure and mechanical properties of Al-Si-Mg alloys. J Mat Process Technol 2004;153-154:193-198.

20. Huang LJ, et al. Effects of hot compression and heat treatment on microstructure and tensile property of Ti-65Al-3.5Mo-1.5Zr-0.3Si alloy. J Mater Sci Eng A 2008;489:330-336.

21. Wang ER, et al. Eutectic Al-Si-Cu-Fe-Mn alloys with enhanced mechanical properties at room and elevated temperature. J Mater Design 2011;32:4333-4340.